Model and Temperature Measurement of Dye-Diffusion Thermal-Transfer Media Scanning Past a Resistive Printhead

Daniel D. Haas, Consultant, Webster, NY, and David A. Johnson, Eastman Kodak Company, Rochester, NY/USA

Abstract: A finite-difference model simulates temperature distributions in two blocks of materials with one block moving with respect to the other block and with a sliding contact region between these blocks. Two different methods of imposing motion with SINDA finite-difference-equation solvers are investigated: SEVER sequentially connects and disconnects different thermal conductors between the two blocks to constitute the sliding contact; SHUTTLE simply marches the temperature profile through the nodes in the moving block at the rate corresponding to the relative speed of the blocks. The SHUTTLE method with integer steps offers the advantage of observing the hottest region in the vicinity of the imaging resistors and the peak temperature at the donor-receiver interface for an arbitrarily long time. Predicted temperatures are confirmed by a 180°C peak temperature experimentally observed at the interface of a 6-μm-thick donor with a paper-backed receiver using the thermal coefficient of electrical resistance (TCR) for a 100-μm-wide silver line deposited on that receiver.

Indexing terms: Conductance, Conductivity, Differential Equation, Donor, Dye-Diffusion Thermal Transfer, Heat Diffusion, Image, Imaging Medium, Ink-sheet, Node, Paper, Printhead, Printing, Receiver, Sever, Silver, Sliding Contact, Shuttle, Specific Heat, Speed, TCR, Temperature, Thermal Coefficient of Resistance, Velocity

Introduction

The temperature profile induced by the heated imaging resistors in a resistive thermal printhead, and throughout the donor and receiver pulled past that printhead, is crucial for determining the amount of dye transferred from the donor to produce the final image density on the receiver. Even if the thermal printer is operated to evolve a steady amount of heat across the length and breadth of the donor with the intent to produce a constant-density image, any one point on the donor or near the top of the receiver experiences rapid heating in a few milliseconds as its location crosses the printhead's heated bead, then cools over a period of tens of milliseconds as the heat deposited by the printhead diffuses deeper into the receiver. During the brief time that the donor dye layer and donor-receiver interface are hotter than the glass-transition temperature of the binder containing dye, that dye can diffuse from donor to receiver. The greater the temperature excursion's magnitude and duration above that glass-transition temperature, the darker the density at that location in the image. The printhead raises its own temperature for at least several seconds while evolving heat at a constant rate, increasing the amount of heat transferred, hence increasing the image density, during printing of an ostensibly constant-density image. Knowledge of the dynamic temperature profile in the printhead, donor, and receiver is needed to improve the design, printing speed, and control of both the printing hardware and the imaging materials.

Tanabe, Asada, and Tsuji [1] have published a two-dimensional finite-element thermal model of the imaging medium moving with respect to the heated printhead, investigating the x-direction of relative motion between printhead and medium and the z-direction proceeding through the layers of the printhead, donor, and receiver. Saquib and Vetterling's two-dimensional finite-difference model of the printhead alone [2, 3] in the x- and y-directions is part of an image-processing algorithm for thermal printing [4, 5]. The y-direction is the dimension along the line of centers of neighboring imaging resistors. Saquib and Vetterling's thermal model accounts for relative motion between the printhead and the imaging medium by treating the arrival of unheated donor as an equivalent static load of a thermal resistance in parallel with a thermal capacitance [3].

Temperature measurements during printing have been reported by using the thermal coefficient of electrical resistance (TCR) of the imaging resistor [6, 7, 8] in the printhead to infer that resistor's temperature several micrometers away from the donor-receiver interface.

Two different techniques, called SEVER and SHUTTLE, applied to the finite-difference solution for the differential equation of heat flow in two and three dimensions will be presented for an imaging medium moving with respect to a heated printhead. Predictions of these techniques will be compared to an analytically solved test case and to experimentally measured temperatures at the donor-receiver interface observed by the TCR of a silver line deposited onto a sheet of receiver.

Two Methods of Imposing Motion on a Finite-Difference Model

Two different techniques are demonstrated for imposing relative motion between the printhead and the imaging medium while providing sliding contact for

thermal conductivity between the printhead and the outer surface of the donor:

SEVER: a sequence of connecting and severing thermal conductors from a static area on the printhead to a small but translating area along the *x*-direction on the back of the donor, as in Figure 1a;

SHUTTLE: shuttling temperatures from each node in the donor to its rightward neighbor along only the *x*-direction while maintaining constant thermal conductance from the static area on the printhead to the static area on the back of the donor, as in Figure 1b.

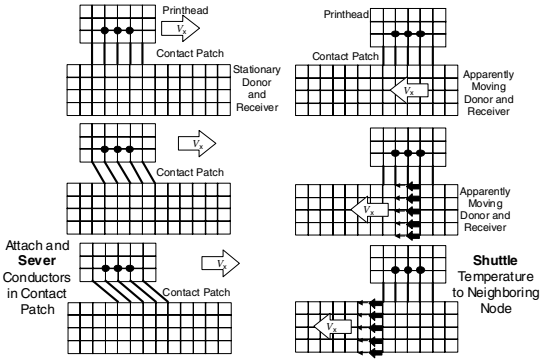

Figure 1: *Two methods of imposing motion on a finite-difference simulation: a) making and SEVERing conductors in the contact patch between printhead and donor; and b) SHUTTLing the temperature profile from one node to the next horizontally through the donor and receiver.*

Connecting and severing thermal conductors performs correctly to produce relative motion of the printhead with respect to donor and receiver in a finite-difference calculation at the expense of some complications in creating the configuration of thermal conductors. The time during which warming by heat transferred from the printhead into the donor-receiver combination can be observed for SEVERing conductors is limited by the length of donor explicitly modeled by the computer program. SHUTTLing temperatures has the advantage of computing the thermal profile in the vicinity of the printhead's contact with the donor, allowing simulation of an arbitrarily long printing session to accommodate the approach of the printhead temperature to its steady state. Both SEVER and SHUTTLE can be implemented using the commercially available SINDA/G [9, 10] finite-difference-solving subroutines.

Motion by Connecting and SEVERing Thermal Conductors

Figure 2 schematizes the two-dimensional model of a rudimentary printhead and donor-receiver combination demonstrating the capability of the first technique of connecting and SEVERing thermal conductors to simulate the thermal behavior for relative motion. The printhead is represented by 12 nodes numbered T106 through T117 in the upper left-hand quadrant of Figure 2, interconnected by 17 thermal conductors numbered G185 through G201. The donor and receiver are represented in the lower half of Figure 2 by 105 nodes numbered T1 through T105 interconnected by 184 thermal conductors numbered G1 through G184.

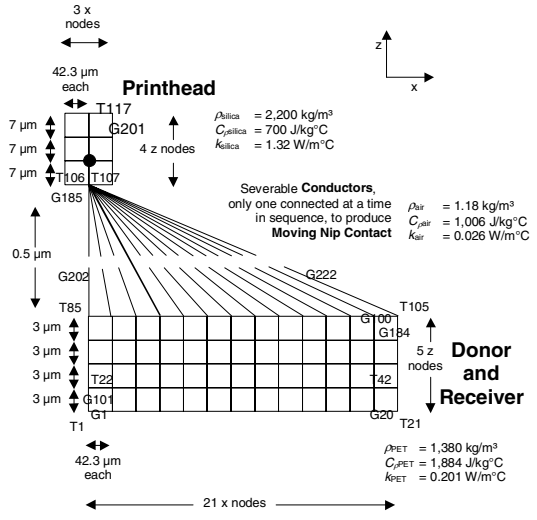

Figure 2: *Rudimentary configuration for imposition of motion on a finite-difference simulation by connecting and severing thermal conductors between a node on a cursory representation of a printhead and a sequence of nodes moving at {V_x = 0.16 m/s} along the outer surface of a crude model of a donor.*

The 21 intervening thermal conductors, all leading from printhead node T107 to the succession of nodes T85 through T105 on the back of the donor, constitute the "contact patch". These 21 conductors, represented by the fan of potential contact-patch thermal conductors G202 through G222 in the center of Figure 2, are created while establishing the configuration during the initial stage of the SINDA finite-difference program. Only one or a small group of these contact-patch conductors G202 through G222 are set to a value of thermal conductance $G(ij)$, the reciprocal of thermal resistance $R(ij)$, typically in units of (W/°C) [9, 10]:

$$G(ij) = \frac{1}{R(ij)} = k\,\frac{[\text{Cross-sectional Area}]}{[\text{Distance between Nodes}]} \qquad (1)$$

while all remaining potential contact-patch conductors are set to zero during any one time step of the solution stage of that SINDA program. k is the thermal conductivity of the material, air in this example, separating the printhead from the outer surface of the donor expressed in units of (W/m°C). As time elapses, the conductor with integer index expressed by Eq. (2) extending from the central node on the bottom surface of the printhead completes contact with a node on the outer surface of the donor.

$$\begin{pmatrix}\text{Index of Thermal Conductor}\\ \text{Connecting Printhead to Donor}\end{pmatrix} = 202 + \text{INT}\left[\frac{t\,V_x}{\Delta x_{node}} + 0.5\right] \quad (2)$$

In Eq. (2):

V_x is the speed of the printhead relative to the donor-receiver combination,

t is the duration of time elapsed between the instant when the middle of the printhead is at the fiducial mark, and the instant of observation,

Δx_{node} is the distance along the x-direction between successive nodes in the donor and receiver.

This sequential conduction to subsequent rightward nodes on the back of the donor imitates the sliding motion of a physical printhead as it contacts and warms advancing donor areas, confirmed by Fig. 3a. The single small white rectangle along the upper edge and to the left of the printhead in Figs. 3a and 3b is a fiducial mark indicating the location of the donor and receiver heated by the printhead at the start of the simulation.

Both the printhead and the donor-receiver combination exhibit anticipated behavior appropriate for sliding contact:

1. The printhead becomes progressively hotter for 24 mW of heat continuously evolved at node 113, with node 107 remaining the coolest because of its loss of heat to the donor;
2. The hottest spot in the donor-receiver combination is always on the back surface of the donor and lags slightly behind the center of the printhead;
3. The hottest spot in the donor-receiver combination attains a higher temperature as the printer runs longer because of the slower heating of the periphery of the printhead;
4. All locations in the donor-receiver combination prior to contact with the printhead remain at ambient temperature;
5. After passage of the printhead, the back of the donor cools principally by conducting heat to deeper locations in the donor and receiver, eventually equalizing the temperature throughout the thickness of the donor and receiver.

Motion by SHUTTLing Temperature to the Neighboring Node

Motion can also be rendered by overwriting the temperature at each node with a temperature shuttled from its neighbor at a previous time, while maintaining the thermal connection from the printhead to the same nodes on the back of the donor, as schematized in Fig. 1b

The simplest application is to shuttle the temperature profile by one node when the donor-receiver combination would have translated that corresponding distance with respect to the printhead. Because the hot spot originates at the stationary printhead on the right side of the temperature profile in Fig. 3b, then propagates with the printhead's relative motion from left to right with respect to the donor and receiver, the temperature profile is shuttled from right to left within the donor and receiver while the printhead appears stationary in Fig. 3b.

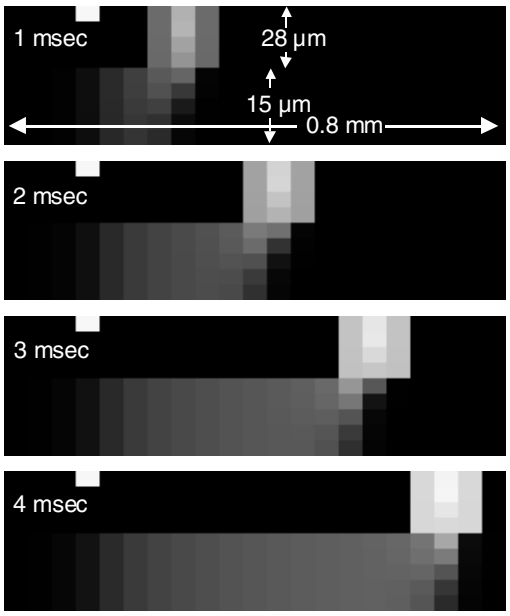

a) SEVER

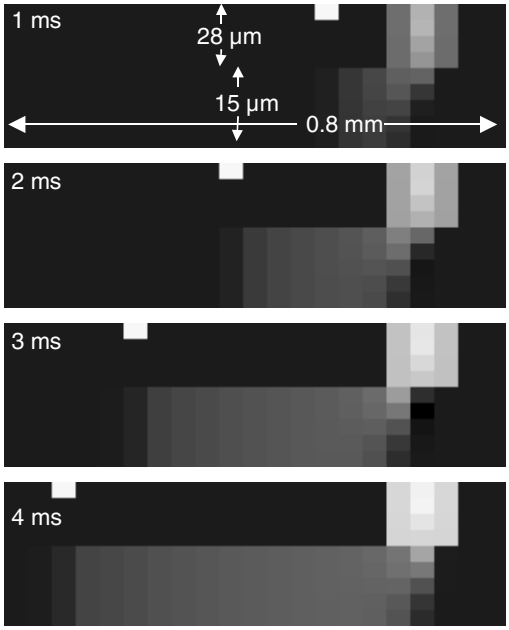

b) SHUTTLE

Figure 3 *Temperature maps for motion imposed on a finite-difference simulation a) by connecting only one thermal conductor while severing all others between one node on the rudimentary printhead and sequence of nodes along the donor's outer surface moving at {V_x = 0.16 m/s}, and b) by shuttling the temperature by a node in synchrony with {V_x = 0.16 m/s} through the donor and receiver while maintaining conductance between a rudimentary printhead and the 4th node along the donor's outer surface. Note that volume elements, called "voxels", are not square in the simulation lattice and that heights change with layer index.*

The stationary printhead at the upper right and the right-to-left movement of the fiducial mark indicating the initially heated segment of donor in each panel in Fig. 3b distinguish the SHUTTLE model from the SEVER model depicting the printhead moving from upper left toward the right in successive panels of Fig. 3a. The general trends of the temperature profiles are identical in the two models.

The SINDA/G finite-difference solver SNDUFR can tolerate SHUTTLing the temperature profile by a node in synchrony with the scanning velocity if the SINDA stability constant CSGFAC is set to less than 0.5. Solver SNADE can tolerate CSGFAC set to 1, and solver SNFRDL can tolerate CSGFAC as large as 5.

Analytical Expression for Quasi-Steady State for a Moving Point Source

A stationary point source in a homogeneous material of infinite extent moving at V_x depicted in Fig. 4 produces a temperature profile [11, 12] plotted in the top panel of Fig. 5:

$$T_{\text{point, quasi-steady state, infinite medium}}[x', y', z'] = \frac{P_{source}}{4\pi k R'} \exp\left[-\frac{V_x}{2A}(R' - x')\right]$$

$$= \frac{P_{source}}{4\pi k\sqrt{(x')^2 + (y')^2 + (z')^2}} \exp\left[-\frac{V_x}{2A}\left(\sqrt{(x')^2 + (y')^2 + (z')^2} - x'\right)\right] \quad (3)$$

in which:

R' is the distance from the point heat source to the location of temperature measurement in the material,

x' is the distance from the point heat source along the direction of motion,

y' is the distance in the material to the side of the heat source,

z' is the depth in the material below the heat source,

k is the thermal conductivity of the material, and

A is the thermal diffusion coefficient of the material.

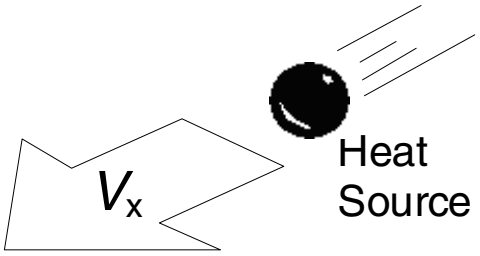

Figure 4 *The quasi-steady-state temperature profile surrounding a point heat source moving through a medium of infinite extent at velocity* V*x can be represented equally well by the temperature in an infinite medium moving at* V*x past a stationary point heat source.*

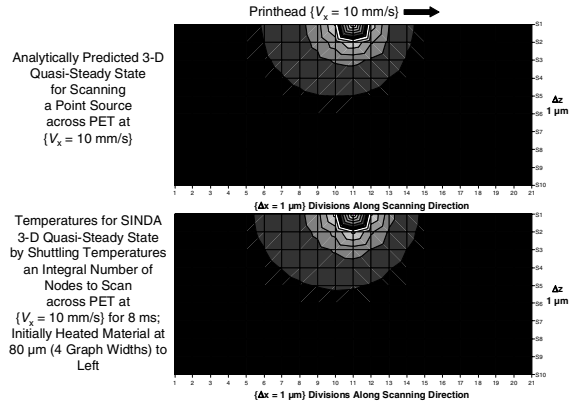

Figure 5 *Central slice through moving-point heat source's three-dimensional temperature contours in the donor by analytical expression (top panel) and by SINDA for SHUTTLing (bottom panel) for both printhead and donor composed of identical material with the same diffusion coefficient. Nodal spacing along the* z*-direction is the same as it is along the* x*-direction, 1 μm.*

Comparison of SINDA Temperature Profiles with a Moving Point Source

The temperature profile in the bottom panel of Fig. 5 is computed by the SINDA program using the SHUTTLE technique for steps through the nodes of the donor and receiver constituted of the same material as the printhead, using the thermal properties listed for the donor and receiver near the bottom of Fig. 2. Only one node evolves heat on the bottom surface of the printhead, which is conducted by only one contact-patch conductance to only one node on the exposed surface of the donor. The finite-difference profile is nearly identical to the analytical result and is distinguishable principally by a slightly larger radius of the dark gray contour near the center of the map.

In order to visualize the small deviations of the SINDA-computed temperatures from the analytical values of Eq. (3) for the moving point heat source, temperature-difference maps are presented as Fig. 6a for SEVER and Fig. 6b for SHUTTLE.

SEVER and SHUTTLE predict nearly identical temperature distributions, with their principal difference occurring far from the heat source where SEVER underestimates the analytical expression less than 2% while SHUTTLE overestimates less than 2%. Both techniques implemented by SINDA generally overestimate the analytical temperature by 30% of an approximation to the volume-averaged peak temperature at the source, by less than 5% of the maximum temperature at nodes neighboring the source, and by less than 1% throughout most of the donor. One instance of about 2% underestimation by both techniques with SINDA/G occurs at a warm node beneath the donor surface just after its passage under the conductor from the printhead.

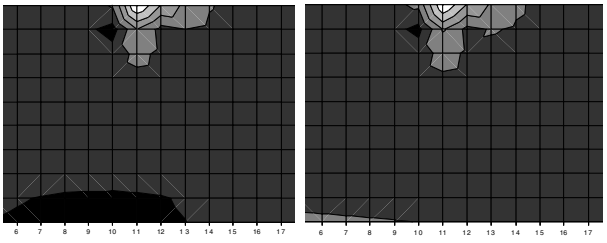

a) SEVER b) SHUTTLE

Figure 6 *Map of temperature differences in the donor for SINDA exceeding the analytical moving-point heat source. Both printhead and donor are composed of identical material with the same diffusion coefficient. Nodal spacing along the z-direction is the same as it is along the x-direction, 1 µm. Dark gray throughout most of the area indicates that the SINDA calculation agrees with the analytical expression to within 1% of peak temperature. Lighter gray indicates SINDA predicts a higher temperature than the analytical expression.*

SINDA Prediction of Temperature History for Experimental Printhead and Imaging Medium

Imposing motion by SHUTTLE for a duration of 300 ms on the SINDA simulation predicts the temperature history depicted as the thin, smooth curve in Fig. 7 experienced by a location at the donor-receiver interface before, during, and after passing under the hot printhead bead. As the location at the donor-receiver interface approaches the hot printhead bead, that location of interest remains at room temperature, assumed to be 20°C in the simulation. Room-temperature medium is moving past the hot printhead bead so fast when printing at (Vx = 0.16 m/s) that negligible heat diffuses through the donor to reach the location of interest until it is under the leading edge of the contact region of the printhead pressing against the outer surface of the donor. The contact region is modeled as 500 µm long with 0.15 µm air space between the printhead bead and the donor surface based upon reflectance-interferometric observations [13]. The temperature at the location of interest rises as fast as 200,000°C/s to a predicted peak of 223°C during a 6-µm-thick donor's brief 1 ms passage under the imaging resistor driven with 32 V pulse-count-modulated at 84% duty cycle to print density near Dmax, as can be appreciated by the steep rise of the left side of the peaked curve in Fig. 7. The speed of the medium is fast enough that negligible heat diffuses to the location of interest after it departs from the back edge of the imaging resistor. Most of the heat in the imaging medium is concentrated in the donor and the top 10 µm of the receiver at this instant of departure. That heat subsequently diffuses vertically through the receiver, cooling the top of the receiver containing the location of interest and warming the lower regions to eventually render the temperature uniform throughout the receiver far from the printing bead. The relative cooling of the location of interest is fast initially and exponentially tapers with time, as seen by the descending arc in the middle and right side of Fig. 7.

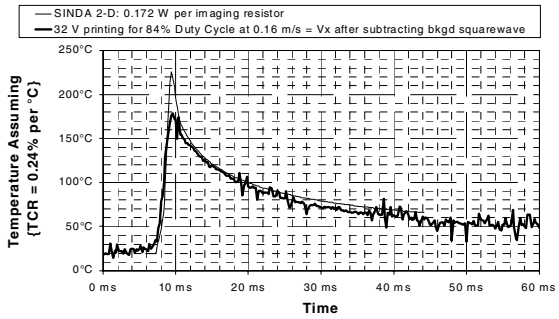

Figure 7*: Temperature predicted by SHUTTLE (thin curve) and measured (thick curve) at the donor-receiver interface under a 6-µm-thick donor support moving {Vx = 0.16 m/s} past a resistive-thermal printhead supplied with pulse-count-modulated 32 V at 84% duty cycle. The measured signal is detected as the rise of electrical resistance of 100-µm-wide, 6,000-Å-thick, 40-mm-long silver line (35.2 Ω at 22°C) on an experimental receiver after removing the squarewave background from the recorded voltage waveform*

Measurement of Temperature Using TCR of a Silver Line Deposited on a Receiver

A 100-µm-wide, 6,000-Å-thick silver line 40 mm long sputtered through a mask onto a paper-backed receiver as depicted in Fig. 8 exhibits a thermal coefficient of resistance of (TCR_{print} = 0.24%/°C) by measurement of that line's electrical resistance in an oven from 20°C to 100°C.

$$R_{print}\left[T_{print}\right] = \left\{1 + \mathrm{TCR}_{print}\left(T_{print} - T_{print,ref}\right)\right\} R_{print}\left[T_{print,ref}\right] \quad (4)$$

This TCR is smaller than the value of 0.41%/°C for bulk pure silver, presumably the result of noncrystallinity of the silver line with a slight contribution caused by the thinness of line [14].

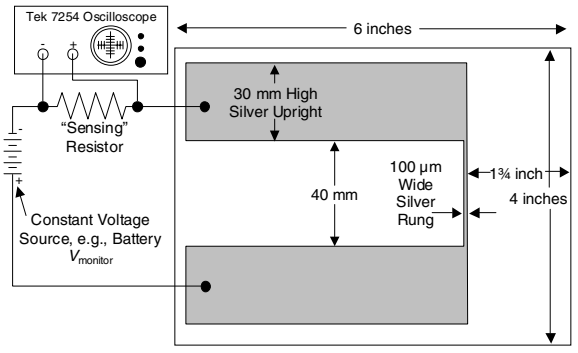

Figure 8*: The change in the heated silver line's electrical resistance can be deduced from the change in current flowing through the sensing resistor, enabling inference of the silver line's temperature.*

The voltage V_{sense} appearing across the "sensing" resistor R_{sense} in the electrical circuit in Fig. 8 is the fraction of the voltage $V_{monitor}$ applied to the entire circuit of resistances R_{sense}, R_{lead} of the leads to the silver line, and R_{print} $[T_{print}]$ of the silver line itself.

$$V_{sense}\left[T_{print}\right] = \frac{R_{sense}}{R_{sense} + R_{leads} + R_{print}\left[T_{print}\right]} V_{monitor} \qquad (5)$$

Substituting Eq. (4) for R_{print} $[T_{print}]$ into Eq. (5) permits rearrangement to find T_{print} of the silver line, using $\{0°C = T_{print,ref}\}$ as a convenient reference temperature for the silver line's resistance:

$$T_{print} = \frac{R_{sense}\left(\frac{V_{monitor}}{V_{sense}\left[T_{print}\right]} - 1\right) - R_{leads} - R_{print,0°C}}{R_{print,0°C}\,\mathrm{TCR}_{print}} + 0°C \qquad (6)$$

Passage of this silver line through the printer under conditions intended to transfer nearly maximum image density to the receiver produces the temperature profile depicted as the thicker solid curve in Fig. 7. This measured temperature profile has been compensated by subtracting a squarewave background with a 1.1 ms period caused by electrical pickup of timing signals radiated by the computer controlling the electrical power sent to the printhead's imaging resistors. Vestiges of this squarewave background can be seen before 8 ms, at about 20 ms, and after 36 ms in the thicker solid curve in Fig. 7.

Predicted peak temperature exceeds measured temperature at the donor-receiver interface by 25%. During the slow decay starting about 10 ms after the peak, the predicted temperature exceeds the measured decaying temperature by about 5%. The greater discrepancy between predicted and observed peak temperatures might be the result of two factors: first, the 100 μm width of the silver line integrates the temperature history over 0.6 ms in Fig. 7, widening and suppressing the peak by about 5°C; and second, inadvertent tilt of the silver line with respect to the line of centers of the imaging resistors in the printhead would subject ends of the silver line to cooler temperatures in front of or behind the hottest strip under the printhead bead, broadening and suppressing the peak by a further 6°C for the first 0.1° of tilt from colinearity.

The raw voltages converted to temperatures for three printing powers corresponding to 32 V (thickest curve), 24 V (thinnest curve), and 15 V (medium-thickness curve) at the same 84% duty cycle of pulse-count modulation and (Vx = 0.16 m/s) printing speed is plotted in Fig. 9 without the removal of the squarewave background. The fact that the observed temperature profile decreases in amplitude in proportion to the square of the voltage applied to the imaging resistors, delineated by a short horizontal line near each peak, confirms that the silver line's electrical signal responds predominantly to temperature and does not exhibit significant pressure sensitivity when compressed by the printhead bead. Pressure sensitivity would have been expected to produce the same electrical signal profile regardless of temperature.

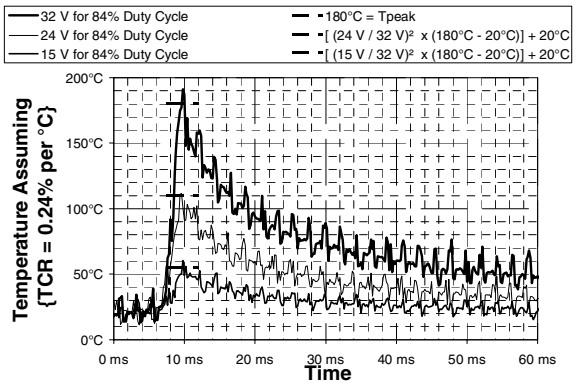

***Figure 9**: Temperature at donor-receiver interface inferred from the raw signal for 6-μm-thick donor moving {V_x = 0.16 m/s} depends upon the electrical voltage (32 V thickest curve, 24 V thinnest curve, and 15 V medium-thickness curve) applied to printhead imaging resistors. The short horizontal lines demarcate the peak temperature scaled according to the square of the voltage, demonstrating that the signal is the result of donor-receiver temperature, not transitory pressure sensitivity of the silver line's electrical resistance during passage through the printing nip.*

Conclusions

The two methods of imposing motion, by SEVERing contact conductors and by SHUTTLing the temperature profile laterally from one node to the next through the imaging materials, implemented with SINDA produce temperature profiles that agree with the analytical expression for a three-dimensional moving point source within 2% for volume elements, called "voxels", separated by more than a node from that source, and within 30% for the volume-average analytical temperature of the voxel containing the point source. SEVER and SHUTTLE produce nearly identical temperature profiles within 0.1% for the refined configuration of each heat source extending over several nodes in the printhead while heating an imaging medium comprising multiple layers of various materials. The computationally simpler method of SHUTTLing the temperature profile possesses the notable advantage of permitting investigation of the imaging region of printhead-donor contact for an arbitrarily long observation time.

Temperature can be measured during printing utilizing the thermal coefficient of electrical resistance of a silver line deposited on one of the imaging materials, without being confounded by pressure sensitivity and without requiring direct optical observation of the sensed location. The value and the dynamics of the observed temperature confirm predictions of both techniques for imposing motion

on the finite-difference thermal model with no adjustable parameters.

Acknowledgments

Gil Hawkins and Christine Landry-Coltrain suggested using the thermal coefficient of electrical resistance of a metal layer as the temperature sensor while printing. Silver lines were vapor-deposited by Mike Culver on a paper-backed receiver through masks obtained by Stan Olshefski and by Frank Jergler. Ed Ozimek provided thermal properties and dimensions of most layers in the printhead and imaging. Mark A. Harris supplied dimensions and thermal properties of components in some of the receiver's layers. Kurt Sanger, Ensley Townsend, Chuck Christ, and Chas Bauer supported and encouraged development of this finite-difference thermal model.

References

[1] F. Tanabe, O. Asada, and K. Tsuji, Electron. Commun. Jpn. Part 2, 72, 76-87 (1989).

[2] S.S. Saquib and W.T. Vetterling, "Model-Based Thermal History Control," NIP 18: 2002 International Conference on Printing Technologies, Society for Imaging Science and Technology, Springfield, VA, pp. 200-204 (2002).

[3] S.S. Saquib and W.T. Vetterling, "A Real-Time Multi-Resolution Algorithm for Correcting Distortions Produced by Thermal Printers," in Proceedings of SPIE-IS&T Electronic Imaging: Computational Imaging III, Vol. 5674, Charles A. Bouman and Eric L Miller, eds., Society of Photo-Optical Instrumentation Engineers, Bellingham, WA, pp. 269-281 (2005).

[4] S.S. Saquib and W.T. Vetterling, "Thermal Response Correction System," U.S. Patent 6,819,347 (2004).

[5] S.S. Saquib and W.T. Vetterling, "Thermal Response Correction System," U.S. Patent Application US2005/0068404 A1 (2005).

[6] T. Kanamori, T. Nakamori, T. Tsuruoka, T. Kitagawa, and S. Shibata, "Optimum Temperature Characteristics of Heat Element Materials for Thermal Transfer Printing," Advanced Printing of the Third International Congress on Advances in Non-Impact Printing Technologies, Society for Imaging Science and Technology, Springfield, VA (1986).

[7] I. Fukushima, "Thermal Head Apparatus," U.S. Patent 5,646,672 (1997).

[8] S.S. Saquib and B. Busch, "Model-Based Estimation of Heating Element Temperature Using Resistance Measurement," 21st International Conference on Digital Printing Technologies Final Program and Proceedings, Society for Imaging Science and Technology, Springfield, VA, pp. 211-214 (2005).

[9] SINDA/G User's Guide, Ver. 2.2, Network Analysis, Inc., 4151 W. Lindbergh Way, Chandler, AZ 85226 (2001), p. 69.

[10] Introducing the SINDA/G Thermal Analyzer: A Tutorial, 12th ed., Network Analysis, Inc., 4151 W. Lindbergh Way, Chandler, AZ 85226 (1998), p. 15.

[11] H.S. Carslaw and J.C. Jaeger, Conduction of Heat in Solids, 2nd Edition (Clarendon Press, Oxford, 1959) pg. 267, Eq. (2).

[12] M. Jakob, Heat Transfer, Vol. 1 (Wiley, New York, 1949) pg. 352, Eq. (17-124).

[13] D. Connolly, J. DeMarco, B. Brock, O. Olson, and M. Robinson, "A Thermal Printing Interferometer," J. Imaging Sci. Technol., 42, 567-571 (1998).

[14] K. Fuchs, "The Conductivity of Thin Metallic Films According to the Electron Theory of Metals," Proceedings of the Cambridge Philosophical Society, 34, 100-108 (1938).

Biography

Dan Haas joined the Research Laboratories at Eastman Kodak Company after completing a Ph.D. thesis on laser doppler velocimetry. He designed reflectometers, fluorimeters, and immunoassays for Kodak's blood analyzer, and computed a phosphor's light-scattering spread function using Boltzmann linear-transport theory. His published theories and measurements explain the digital-printing artifacts of banding and contouring. He developed an analytical model to calculate donor heating by a laser in the Kodak Approval digital color imaging system and a numerical model for donor heating in dye-diffusion thermal-transfer printers. Subsequent to measuring temperatures during resistive-head thermal printing, Dr. Haas has become an independent consultant.

David Johnson joined Eastman Kodak Company after receiving a B.S. in Electrical Engineering from the University of Wyoming. He has extensive experience in the design and testing of thermal dye-diffusion printers, ink-jet printers, and xenon flash illumination systems. He has worked with several manufacturers of thermal print heads to specify, characterize, and improve the performance of their printheads in dye diffusion printing applications.